A Lithium-Ion Battery-in-the-Loop Approach to Test and Validate Multiscale Dual H Infinity Filters for State-of-Charge and Capacity Estimation

Cheng Chen, Rui Xiong, *Senior Member, IEEE*, and Weixiang Shen, *Member, IEEE*

***Abstract*—An accurate battery capacity and state estimation method is one of the most significant and difficult techniques to ensure efficient and safe operation of the batteries for electric vehicles (EVs). Since capacity and state of charge (SoC) are strongly correlated, the SoC is hardly to be accurately estimated without knowing accurate battery capacity. Thus, a multiscale dual H infinity filter (HIF) has been proposed to estimate battery SoC and capacity in real time with dual timescales in response to slow-varying battery parameters and fast-varying battery state. The proposed method is first evaluated and verified using off-line experimental data and then compared with the single/multiscale dual Kalman filters (KFs). The results show that the proposed multiscale dual HIFs has better robustness and higher estimation accuracy than the single/multiscale dual KFs. To further validate the feasibility of the proposed method for EV applications, a lithium-ion battery-in-the-loop approach is applied to verify the stability and accuracy of the SoC estimation, and it is found that the SoC estimated from the proposed method can converge to the reference value gradually and be stabilized within 2%.**

***Index Terms*—Battery in the loop, capacity, dual H infinity filters (HIFs), lithium-ion battery, multiscale, state of charge (SoC).**

I. Introduction

With the superiority of high specific energy and specific power, lithium-ion batteries are widely used in the development of electric vehicles (EVs) [1], [2]. For safe and efficient operation of EVs, it is essential for battery management systems to accurately estimate the state of charge (SoC) and capacity so that batteries can be balanced and managed effectively in EVs [3], [4]. However, the estimation of battery SoC and capacity is challenging in uncertain and complex EV environments.

There are various SoC estimation methods. They can generally be divided into four categories: lookup table methods [5], ampere–hour methods [6], model-based methods [7]–[9], and data-driven methods, including neural networks [10], fuzzy controllers [11], and support vector regressions [12]. Among them, the model-based methods provide the robust performance for the SoC estimation due to their sustained error correction mechanism through the closed-loop feedback. In [7], the Thevenin model is combined with the Lyapunov-based adaptive observer to obtain the accurate SoC. In [8], the dual polarization (DP) model is used to estimate the SoC based on the particle swarm optimization (PSO). In [9], the resistance–capacitance (*RC*) model with the nonlinear characteristics of SoC versus open-circuit voltage (OCV) for Li-PB is used to estimate the SoC with the sliding-mode observer. Obviously, the state estimation algorithm and the battery model are the keys of the SoC estimation. For the former, the Kalman filter (KF) and its improved forms are typically the representative algorithms. The extended KF (EKF) shows a good estimation of the SoC with a fast convergence at erroneous initial values of SoCs in [10]. The unscented KF (UKF) is proved to have higher estimation precision and less computational burden than the EKF due to its no requirement of linearizing nonlinear model in [13]. The adaptive UKF (AUKF) whose process and measurement noise covariance can be adjusted adaptively in the estimation process is proposed to obtain more accurate results than the UKF in [14]. As a general rule, the KFs can minimize the covariance of the estimation error based on the assumptions of accurate battery models and known statistical characteristics of noises, so they do not make any guarantee of estimation error when the assumptions are not met in the actual process. The H infinity filter (HIF) based on the minimax error criterion, which is proposed and improved in [15] and [16], can still guarantee estimation accuracy in the worst case, and it is increasingly popular in the field of state estimation [17]–[20]. The experimental results of the SoC estimation in [21] show that the HIF can provide the accurate SoC estimation at inexact or unknown statistical properties of the errors. Furthermore, the adaptive algorithms for estimating noise covariance matrices are introduced in [22]. In [23], the mixed Kalman/H-infinity filtering approach is proved to have better performance than either of the algorithms individually. For the latter, battery model parameters significantly

Manuscript received September 14, 2016; revised December 2, 2016; accepted February 9, 2017. Date of publication February 16, 2017; date of current version October 6, 2017. This work was jointly supported by the National Natural Science Foundation of China under Grant 51507012, by the Australian Research Council Linkage Grant under Grant LP110200302, by the Sino-Polish Collaborative Research in E-mobility Public Transportation under Grant 2015DFG81930, by the Beijing Nova Program under Grant Z171100001117063, and by the Joint Funds of the National Natural Science Foundation of China under Grant U1564206. Recommended for publication by Associate Editor F. H. Khan. *(Corresponding author: Rui Xiong)*

C. Chen and R. Xiong are with the National Engineering Laboratory for Electric Vehicles, School of Mechanical Engineering, Beijing Institute of Technology, Beijing 100081, China, and also with the Collaborative Innovation Center of Electric Vehicles in Beijing, Beijing Institute of Technology, Beijing 100081, China (e-mail: chencheng@bit.edu.cn; rxiong@bit.edu.cn).

W.X. Shen is with the Faculty of Science, Engineering, and Technology, Swinburne University of Technology, Hawthorn, Vic. 3122, Australia (e-mail: wshen@swin.edu.au).

Color versions of one or more of the figures in this paper are available online at http://ieeexplore.ieee.org.

Digital Object Identifier 10.1109/TPEL.2017.2670081

affect estimation performances, off-line identification of battery parameters is not appropriate when the working environment of batteries is changing. For the practical applications in EVs, online identification of battery parameters is proposed to update battery parameters regularly in [24] and [25], such as a moving-window least square method in [25], which leads to the exploration of the joint estimation of battery states and parameters such as a recursive least square (RLS) and an AEKF in [26]. Since the RLS and the AEKF are independent modules in this method, it is hard to ensure its convergence. In [27], the combination of state estimation and parameter identification is used to estimate the SoC and state of energy. The experimental results show good accuracy and robustness.

In addition, the model-based methods usually obtain the SoC state equation through an ampere–hour counting method, where battery capacity is assumed to be a known parameter but actually changing slowly with aging. To overcome this problem, many methods have been investigated to estimate battery capacity in real time [28]–[31]. The OCV is utilized to obtain the accurate SoC, which is then used to calculate the battery capacity online [28], [29]. The accuracy of the calculated capacity depends on the current, which is difficult to be measured accurately in EV environments. In [30], the degradation models are established to estimate battery capacity based on a series of experimental data, which is very time consuming. In [31], battery capacity is considered as a system parameter and then a dual EKF is proposed to estimate the SoC and capacity online. However, fast-varying states (e.g., SoC) and slow-varying parameters (e.g., capacity) require dual estimation methods in different timescales [32], [33], which will not only increase the stability of the estimation methods but also reduce their computation complexity.

Based on this rationale, this paper uses the HIF to construct a multiscale dual HIF for the SoC and capacity estimation. To further verify the reliability and accuracy of the proposed multiscale dual HIF for the SoC and capacity estimation, the battery-in-loop test based on xPC target [34] is set up to closely simulate EV operation environments for a real-time validation [35], [36].

The rest of this paper is organized as follows. The description of a discrete-time nonlinear system and the multiscale dual HIF are presented in Section II. Section III describes the implementation of the multiscale dual HIF in battery systems for the SoC and capacity estimation. The experimental and simulation results as well as the evaluation of the multiscale dual HIF algorithm are reported in Section IV. Section V further verifies the multiscale dual HIF algorithm by the battery-in-loop test, followed by the conclusions drawn in Section VI.

II. Multiscale Dual HIFs

In this section, the HIF and the single-scale dual HIF are first introduced as a preparation. Then, the multiscale dual HIF is proposed to estimate system states and parameters based on the multiscale discrete-time nonlinear system.

A. HIFs and Single-Scale Dual HIFs

Based on the principle of minimizing the maximum estimation error, the HIF ensures the good estimation performance even in the worst case, and it defines cost function as follows:

$$J_1 = \frac{\sum_{k=0}^{N-1} \|x_k - \hat{x}_k\|_{S_k}^2}{\|x_0 - \hat{x}_0\|_{P_0^{-1}}^2 + \sum_{k=0}^{N-1} \left(\|w_k\|_{Q_k^{-1}}^2 + \|v_k\|_{R_k^{-1}}^2 \right)} \quad (1)$$

where x_k is the system state and $\hat{x}_k$ is its guess value; x_0 is the initial system state and $\hat{x}_0$ is its guess value; w_k is the process noise vector for system states; v_k is the measurement noise vector; P_0, Q_k, R_k, and S_k are the symmetric positive definite matrices that should be chosen by designers based on the specific applications. According to the mathematical deduction in [15] and [16], the following recursive filtering algorithm is obtained:

$$\begin{cases} K_k = P_k \left(I - \delta S_k P_k + C_k^{\mathrm{T}} R_k^{-1} C_k P_k\right)^{-1} C_k^{\mathrm{T}} R_k^{-1} \\ \hat{x}_{k+1} = A_k \hat{x}_k + A_k K_k \left(y_k - C_k \hat{x}_k\right) \\ P_{k+1} = A_k P_k \left(I - \delta S_k P_k + C_k^{\mathrm{T}} R_k^{-1} C_k P_k\right)^{-1} A_k^{\mathrm{T}} + Q_k \end{cases} \quad (2)$$

where δ is the performance boundary designed by users; A_k and C_k are the coefficient matrices; P_k is obtained by recursive operation from P_0; and K_k is the gain matrix at time t_k.

The HIF estimates the states while providing the uncertainty vector of the states which indicates the error bounds of the estimated states. Three confidence levels of 65.3%, 95.4%, and 99.7% are very commonly adopted in practical applications. The confidence level of 65.3% will cause the loss of high-confidence results, while the confidence level of 99.7% will bring about the overmuch low-confidence results. Thus, this paper selects the confidence level of 95.4%, which means we are 95.4% confident that the true state x_k will be bounded by $\hat{x}_k \pm 2\sqrt{\mathrm{diag}(\Sigma_k)}$, where Σ_k is the error covariance of state, which is expressed by

$$\Sigma_k = (I - K_k C_k)\Sigma_{k-1}(I - K_k C_k)^T + K_k R_k K_k^T. \quad (3)$$

To achieve dual estimation of states and parameters, the procedure includes states update prepared for parameter identification and parameters update that is premise of state estimation, which is summarized in Table I.

The system parameters C_k^θ in (5) are the function of the system states and can be calculated by

$$C_k^\theta = \frac{dg\left(x_k, \theta, u_k\right)}{d\theta} = \frac{\partial g(x_k, u_k, \theta)}{\partial \theta} + \frac{\partial g(x_k, u_k, \theta)}{\partial x_k} \frac{dx_k}{d\theta} \quad (12)$$

where

$$\frac{dx_k}{d\theta} = \frac{\partial f(x_{k-1}, u_{k-1}, \theta)}{\partial \theta} + \frac{\partial f(x_{k-1}, u_{k-1}, \theta)}{\partial x_{k-1}} \frac{dx_{k-1}}{d\theta}. \quad (13)$$

The derivative calculations are recursive in nature and evolve over time. The term $dx_0/d\theta$ is initialized to zero unless the priori information gives a better estimate of its value. This algorithm is initialized by providing the system states and parameters, the matrices and performance boundary to the best guesses based on the prior information.

TABLE I
ALGORITHM OF SINGLE-SCALE DUAL HIFS

Nonlinear System

$$\begin{cases} x_k = f(x_{k-1}, \theta_{k-1}, u_{k-1}) + w_{k-1} \\ \theta_k = \theta_{k-1} + \rho_{k-1} \\ y_k = g(x_k, \theta_k, u_k) + v_k \end{cases} \tag{4}$$

Definition

$$A_{k-1} = \left.\frac{df(x, \hat{\theta}_k^-, u_{k-1})}{dx}\right|_{x_k = \hat{x}_{k-1}^+}, C_k^x = \left.\frac{dg(x, \hat{\theta}_k^-, u_k)}{dx}\right|_{x_k = \hat{x}_k^-}$$
$$C_k^\theta = \left.\frac{dg(\hat{x}_k^+, \theta, u_k)}{d\theta}\right|_{\theta_k = \hat{\theta}_k^-} \tag{5}$$

Initialization

$$\hat{x}_0 = E(x_0),\ P_0^x = E\left[(x_0 - \hat{x}_0)(x_0 - \hat{x}_0)^T\right] \tag{6}$$
$$\hat{\theta}_0 = E(\theta_0),\ P_0^\theta = E\left[(\theta_0 - \hat{\theta}_0)(\theta_0 - \hat{\theta}_0)^T\right] \tag{7}$$

where θ_k is the system parameter and $\hat{\theta}_k$ is its guess value; θ_0 is the initial system parameter and $\hat{\theta}_0$ is its guess value.

For $k \in \{1, 2, \ldots, \infty\}$, do the following calculation:

Step 1: Time-update equations for parameters

$$\hat{\theta}_k^- = \hat{\theta}_{k-1}^+,\ P_k^{\theta,-} = P_{k-1}^{\theta,+} + Q_{k-1}^\theta \tag{8}$$

Step 2: Time-update equations for states

$$\hat{x}_k^- = f(\hat{x}_{k-1}^+, \hat{\theta}_k^-, u_{k-1}),\ P_k^{x,-} = A_{k-1} P_{k-1}^{x,+} A_{k-1}^{\mathrm{T}} + Q_{k-1}^x \tag{9}$$

Step 3: Measurement-update equations for states

$$\begin{cases} e_k^x = y_k - g(\hat{x}_k^-, \hat{\theta}_k^-, u_k) \\ K_k^x = P_k^{x,-}(I - \delta_x S_k^x P_k^{x,-} + (C_k^x)^{\mathrm{T}}(R_k^x)^{-1} C_k^x P_k^{x,-})^{-1} \\ \quad \times (C_k^x)^{\mathrm{T}}(R_k^x)^{-1} \\ \hat{x}_k^+ = \hat{x}_k^- + K_k^x e_k^x \\ P_k^{x,+} = P_k^{x,-}(I - \delta_x S_k^x P_k^{x,-} + (C_k^x)^{\mathrm{T}}(R_k^x)^{-1} C_k^x P_k^{x,-})^{-1} \end{cases} \tag{10}$$

Step 4: Measurement-update equations for parameters

$$\begin{cases} e_k^\theta = y_k - g(\hat{x}_k^+, \hat{\theta}_k^-, u_k) \\ K_k^\theta = P_k^{\theta,-}(I - \delta_\theta S_k^\theta P_k^{\theta,-} + (C_k^\theta)^{\mathrm{T}}(R_k^\theta)^{-1} C_k^\theta P_k^{\theta,-})^{-1} \\ \quad \times (C_k^\theta)^{\mathrm{T}}(R_k^\theta)^{-1} \\ \hat{\theta}_k^+ = \hat{\theta}_k^- + K_k^\theta e_k^\theta \\ P_k^{\theta,+} = P_k^{\theta,-}(I - \delta_\theta S_k^\theta P_k^{\theta,-} + (C_k^\theta)^{\mathrm{T}}(R_k^\theta)^{-1} C_k^\theta P_k^{\theta,-})^{-1} \end{cases} \tag{11}$$

B. Multiscale Dual HIFs

The dual HIF provide the dual estimation of states and parameters. In general, the states show the fast-varying characteristic and the parameters show the slow-varying characteristic. The following equation describes a multiscale discrete-time nonlinear system:

$$\begin{cases} x_k = f(x_{k-1}, \theta_l, u_{k-1}) + w_{k-1} \\ \theta_l = \theta_{l-L} + \rho_{l-L} \\ y_k = g(x_k, \theta_l, u_k) + v_k \end{cases} \tag{14}$$

where k indicates the timescale for system state estimation accomplished at the sampling time t_k, and here, $k = 0,\ 1,\ 2, \ldots$; x_k is the system state vector at the time t_k; l indicates the timescale for system parameter estimation accomplished at the sampling time t_l, and here, $l = L,\ 2L,\ 3L, \ldots$ (L is the limit value for scale conversion); θ_l is the system parameter vector updated at the time t_l, which will be used to estimate system states between the time t_{l+1} and t_{l+L} and $l = 0$ means the initial value of the parameter, as shown in Fig. 1; u_k is the system input vector at time t_k;ρ_l is the process noise vector for system parameters; and y_k is the system measurement vector at time t_k.

Therefore, the single-scale dual HIF in Table I is improved as the multiscale dual HIF to estimate system states and parameters with different timescales as summarized in Table II.

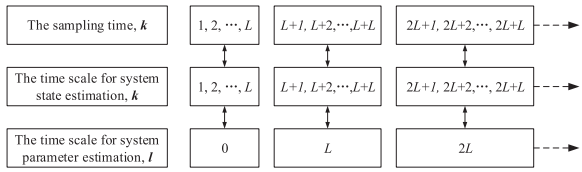

Fig. 1. Timescales for state and parameter estimation.

TABLE II
ALGORITHM OF MULTISCALE DUAL HIFS

Nonlinear System

$$\begin{cases} x_k = f(x_{k-1}, \theta_l, u_{k-1}) + w_{k-1} \\ \theta_l = \theta_{l-L} + \rho_{l-L} \\ y_k = g(x_k, \theta_l, u_k) + v_k \end{cases}$$

Definition

$$A_{k-1} = \left.\frac{df(x, \hat{\theta}_k^-, u_{k-1})}{dx}\right|_{x_k = \hat{x}_{k-1}^+}, C_k^x = \left.\frac{dg(x, \hat{\theta}_k^-, u_k)}{dx}\right|_{x_k = \hat{x}_k^-}$$
$$C_l^\theta = \left.\frac{dg(\hat{x}_k^+, \theta, u_k)}{d\theta}\right|_{\theta_l = \hat{\theta}_l^-} \tag{15}$$

Initialization: install L and l(here $l = 0$)

$$\hat{x}_0^+ = E(x_0),\ P_0^{x,+} = E\left[(x_0 - \hat{x}_0)(x_0 - \hat{x}_0)^T\right] \tag{16}$$
$$\hat{\theta}_0^+ = E(\theta_0),\ P_0^{\theta,+} = E\left[(\theta_0 - \hat{\theta}_0)(\theta_0 - \hat{\theta}_0)^T\right] \tag{17}$$

For $k \in \{1, 2, \ldots, \infty\}$, do the following calculation:

Step 1: Time-update equations for state

$$\hat{x}_k^- = f(\hat{x}_{k-1}^+, \hat{\theta}_l^+, u_{k-1}),\ P_k^{x,-} = A_{k-1} P_{k-1}^{x,+} A_{k-1}^T + Q_{k-1}^x \tag{18}$$

Step 2: Measurement-update equations for state

$$\begin{cases} e_k^x = y_k - g(\hat{x}_k^-, \hat{\theta}_l^+, u_k) \\ K_k^x = P_k^{x,-}(I - \delta_x S_k^x P_k^{x,-} + (C_k^x)^T (R_k^x)^{-1} C_k^x P_k^{x,-})^{-1} \\ \quad \times (C_k^x)^T (R_k^x)^{-1} \\ \hat{x}_k^+ = \hat{x}_k^- + K_k^x e_k^x \\ P_k^{x,+} = P_k^{x,-}(I - \delta_x S_k^x P_k^{x,-} + (C_k^x)^T (R_k^x)^{-1} C_k^x P_k^{x,-})^{-1} \end{cases} \tag{19}$$

Step 3: Judge whether k divided by L with no remainder. If so, make $l = l + L$ and continue to step 4; otherwise, return to step 1 and get ready for the calculation of next sampling time.

Step 4: Time-update equations for parameters

$$\hat{\theta}_l^- = \hat{\theta}_{l-L}^+,\ P_l^{\theta,-} = P_{l-L}^{\theta,+} + Q_{l-L}^\theta \tag{20}$$

Step 5: Measurement-update equations for parameters

$$\begin{cases} e_l^\theta = y_k - g(\hat{x}_k^+, \hat{\theta}_l^-, u_k) \\ K_l^\theta = P_l^{\theta,-}(I - \delta_\theta S_l^\theta P_l^{\theta,-} + (C_l^\theta)^{\mathrm{T}}(R_l^\theta)^{-1} C_l^\theta P_l^{\theta,-})^{-1} \\ \quad \times (C_l^\theta)^{\mathrm{T}}(R_l^\theta)^{-1} \\ \hat{\theta}_l^+ = \hat{\theta}_l^- + K_l^\theta e_l^\theta \\ P_l^{\theta,+} = P_l^{\theta,-}(I - \delta_\theta S_l^\theta P_l^{\theta,-} + (C_l^\theta)^{\mathrm{T}}(R_l^\theta)^{-1} C_l^\theta P_l^{\theta,-})^{-1} \end{cases} \tag{21}$$

III. APPLICATION TO BATTERY SYSTEMS

A. Battery Model

It is important to select a suitable model for the application of the earlier methods. There are many battery models, such as Rint model, *RC* model, the Thevenin model, and the Partnership for a New Generation of Vehicles (PNGV) model. Among them, the Thevenin model is widely used because of its balance between simplicity and accuracy [7], [26], [31]. So, the Thevenin model is selected in this study and its equivalent circuit is shown in Fig. 2.

According to circuit theory, this battery model can be described by

$$\begin{cases} U_t = U_{oc} - U_p - i_L R_0 \\ \dot{U}_p = -\dfrac{1}{C_p R_p} U_p + \dfrac{1}{C_p} i_L \end{cases} \tag{22}$$

where U_t is the terminal voltage; U_{oc} is the OCV; U_p is the polarization voltage and $\dot{U}_p$ is the time derivative of U_p; i_L is

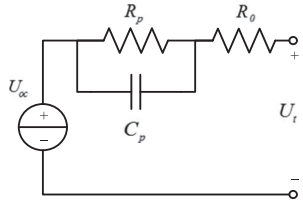

Fig. 2. Thevenin model of a battery.

the current; R_0 is the ohmic internal resistance; and C_p and R_p are the polarization capacitance and resistance, respectively.

Considering slow-varying behaviors of a battery, we assume that the battery is a time-invariant system and the load current is constant at each sampling interval. As a result, (22) can be converted into a difference equation by standard techniques, where the discrete-time battery model is modified to a multiscale model as

$$\begin{cases} U_{p,k+1} = \exp\left(\dfrac{-\Delta t}{C_{p,l}R_{p,l}}\right)U_{p,k} + \left[1-\exp\left(\dfrac{-\Delta t}{C_{p,l}R_{p,l}}\right)\right] i_{L,k}R_{p,l} \\ U_{t,k} = U_{oc,k} - U_{p,k} - i_{L,k}R_{0,l} \end{cases} \tag{23}$$

where Δt is the sampling period, and its value approximates to be 1 s in this paper. According to the ampere–hour counting method, the SoC state equation can be described as a discrete-time form

$$z_{k+1} = z_k - \frac{\eta\left(i_{L,k}\right) i_{L,k}\Delta t}{C_{a,l}} \tag{24}$$

where z_k is the SoC at the time t_k, $i_{L,k}$ is the load current at time t_k, $\eta(i_{L,k})$ is the coulomb efficiency of the battery, and $C_{a,l}$ is the battery capacity, which is a function of temperature and aging level [37], [38]. Together with the model parameters in (23), $C_{a,l}$ is considered as a system parameter and will be updated at the time $t_{l\times L}$, where the subscript $l \times L$ means the sampling period for the battery capacity.

The relatively stable SoC–OCV curve is usually used to calibrate battery SoC. In fact, this curve is affected by temperature and aging to a certain extent, which mainly reflects in the change of battery capacity [37], [38]. To tackle the capacity change, the capacity–SoC–OCV curve surface can be used in the measurement-update process of SoC and capacity, and it is obtained by the following equations.

First, the OCV can be described by an electrochemical equation

$$\begin{aligned} U_{oc,k}\left(C_{a,l}, z_k\right) = {} & \alpha_0 + \alpha_1 z_k + \alpha_2 z_k^2 + \alpha_3 z_k^3 + \alpha_4/z_k \\ & + \alpha_5 ln\left(z_k\right) + \alpha_6 \ln\left(1 - z_k\right) \end{aligned} \tag{25}$$

where the coefficients of (25) are defined as the quadratic function of capacity as

$$\left[\alpha_0\ \alpha_1\ \alpha_2\ \alpha_3\ \alpha_4\ \alpha_5\ \alpha_6\right]^{\mathrm{T}} = \Lambda \times \left[C_{a,l}^2\ C_{a,l}\ 1\right]^{\mathrm{T}} \tag{26}$$

where $\alpha_0, \alpha_1, \alpha_2, \alpha_3, \alpha_4, \alpha_5, \alpha_6$ are the coefficients in the electrochemical equation and Λ is a constant matrix and is obtained by the experimental data.

Up to now, we have the system state vector x_k and parameter vector θ_l

$$x_k = \left[U_{p,k}\ z_k\right]^T \tag{27}$$

$$\theta_l = \left[R_{0,l}\ R_{p,l}\ C_{p,l}\ C_{a,l}\right]^T \tag{28}$$

Combining (23) and (24) yields the state and measurement equations as follows:

$$\begin{cases} x_{k+1} = f\left(x_k, \theta_l, u_k\right) = \begin{bmatrix} \exp\left(\dfrac{-\Delta t}{C_{p,l}R_{p,l}}\right) & 0 \\ 0 & 1 \end{bmatrix} x_k \\ \quad + \begin{bmatrix} [1 - \exp\left(\dfrac{-\Delta t}{C_{p,l}R_{p,l}}\right)] i_{L,k}R_{p,l} \\ \eta\left(i_{L,k}\right) i_{L,k}\Delta t / C_{a,l} \end{bmatrix} \\ y_k = g\left(x_k, \theta_l, u_k\right) = U_{oc,k} - U_{p,k} - R_{0,l}i_{L,k} \end{cases} \tag{29}$$

where $y_k = U_{t,k}$, which is the battery terminal voltage, and $u_k = i_{L,k}$, which is the battery current.

B. Implementation of Multiscale Dual HIFs in Battery Systems

According to the multiscale dual HIF shown in Table II, we estimate the battery state vector with the known battery parameters, current, and terminal voltage and then use the new state vector to update the parameter vector. Because the battery states and parameters have different changing rates, we can update those values in different timescales.

From (15), (25), and (29), we obtain all the matrices and observation equations as

$$A_{k-1} = \begin{bmatrix} \exp\left(\dfrac{-\Delta t}{C_{p,l}R_{p,l}}\right) & 0 \\ 0 & 1 \end{bmatrix} \tag{30}$$

$$C_k^x = \left[-1\ \frac{\partial U_{oc}\left(C_{a,l}, z_k\right)}{\partial z}\Big|_{z=\hat{z}_k^-} \right]^T \tag{31}$$

$$\begin{aligned} C_l^\theta = {} & \left[-i_{L,k}\ 0\ 0\ \frac{\partial U_{oc}(C_a, z)}{\partial C_a}\Big|_{C_a=\hat{C}_{a,l}^-, z=\hat{z}_k^+} \right]^T \\ & + C_k^x \frac{\partial x_k}{\partial \theta}\Big|_{\theta=\hat{\theta}_l^-, x=\hat{x}_k^+} \end{aligned} \tag{32}$$

where

$$\frac{\partial U_{oc}}{\partial z} = \alpha_1 + 2\alpha_2 z + 3\alpha_3 z^2 - \alpha_4/z^2 + \alpha_5/z - \alpha_6/\left(1 - z\right) \tag{33}$$

$$\begin{aligned} \frac{\partial U_{oc}}{\partial C_a} = {} & \left[\ 1\ z\ z^2\ z^3\ 1/z\ \ln\left(z\right)\ \ln\left(1 - z\right)\right] \\ & \times \Lambda \times \left[2C_a \quad 1 \quad 0\right] \end{aligned} \tag{34}$$

$$\frac{dx_k}{d\theta} = \frac{\partial f(x_{k-1}, u_{k-1}, \theta)}{\partial \theta} + A_{k-1}\frac{dx_{k-1}}{d\theta} \tag{35}$$

$$\frac{\partial f(x_{k-1}, u_{k-1}, \theta)}{\partial \theta} = \begin{bmatrix} 0 & b_1 & b_2 & 0 \\ 0 & 0 & 0 & b_4 \end{bmatrix} \tag{36}$$

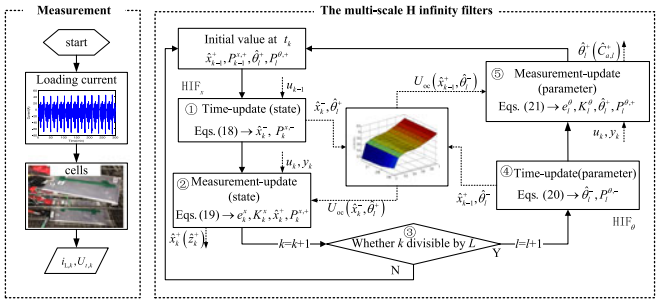

Fig. 3. Implementation flowchart of multiscale dual HIFs.

$$\begin{cases} b_1 = \dfrac{U_{p,k-1}\Delta t}{R_{p,l}^2 C_{p,l}} \exp\left(\dfrac{-\Delta t}{C_{p,l}R_{p,l}}\right) - \dfrac{i_{L,k-1}\Delta t}{C_{p,l}R_{p,l}} \exp\left(\dfrac{-\Delta t}{C_{p,l}R_{p,l}}\right) \\ -i_{L,k}\left[\exp\left(\dfrac{-\Delta t}{C_{p,l}R_{p,l}}\right) - 1\right] \\ b_2 = \dfrac{U_{p,k-1}\Delta t}{C_{p,l}^2 R_{p,l}} \exp\left(\dfrac{-\Delta t}{C_{p,l}R_{p,l}}\right) - \dfrac{i_{L,k-1}\Delta t}{C_{p,l}^2} \exp\left(\dfrac{-\Delta t}{C_{p,l}R_{p,l}}\right) \\ b_4 = \dfrac{\eta\left(i_{L,k}\right) i_{L,k}\Delta t}{C_{a,l}^2} \end{cases} \tag{37}$$

Fig. 3 shows the implementation flowchart of the multiscale dual HIF in Table II. The detailed implementation procedure is explained as follows.

While the batteries are discharging, the current and terminal voltage of the batteries are measured in real time by their corresponding sensors through the low-pass filter modules, and these measured data transmits to the multiscale dual HIF to execute the dual estimation which can be shown in the following five steps:

1) Based on the initial value settings at the time t_k, HIF$_x$ executes the time update and calculates the *a priori* parameter estimation $\hat{x}_k^-$ and the matrix $P_k^{x,-}$ by (18). This step prepares for the next state estimation.
2) After the time update of HIF$_x$, the estimated terminal voltage at the time t_k is obtained. The error between the estimated and measured terminal voltages is used to execute the measurement update of HIF$_x$ by the correction of gain matrix, where the *a posteriori* state estimation $\hat{x}_k^+(\hat{z}_k^+)$ and the matrix $P_k^{x,+}$ are computed by (19). In this step, the optimal state estimation at the time t_k is used to calculate the *a priori* state at the next time.
3) Judge whether k divided by L with no remainder. If so, make $l = l + L$ and continue to step 4); otherwise, return to step 1) and get ready for the calculation of next sampling time.
4) On the basis of step 2), HIF$_\theta$ executes the time update and calculates the *a priori* parameter estimation $\hat{\theta}_l^-$ and the matrix $P_l^{\theta,-}$ by (20). This step prepares for the next parameter estimation.
5) After the time update of parameter estimation, HIF$_\theta$ is ready to execute the measurement update with the *a posteriori* state estimation and *a priori* parameter estimation at time t_l. Then, we obtain the *a posteriori* state estimation $\hat{\theta}_l^+(\hat{C}_{a,l}^+)$ and the matrix $P_l^{\theta,+}$ calculated by (21), which will return to step 1) and get ready for the calculation of next sampling time.

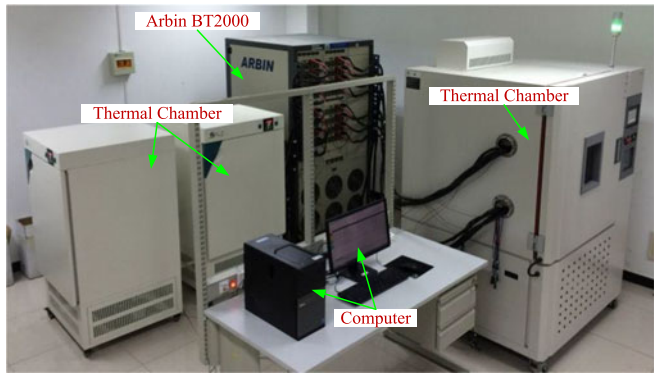

Fig. 4. Physical map of battery test bench.

There are totally 12 design parameters, including $\hat{x}_0$, P_0^x, Q_k^x, R_k^x, δ_x, S_k^x in the state estimation module and $\hat{\theta}_0$, P_0^θ, Q_k^θ, R_k^θ, δ_θ, S_k^θ in the parameter estimation module. $\hat{x}_0$ is the initial state vector including the initial SoC and the initial polarization voltage. In this study, the initial SoC is set to 0.8 for the fully charged battery and the initial polarization voltage is set to 0. P_0^x is a 2×2 symmetric positive definite matrix. The initial values of $P_0^x(i,i)$ are set correspondingly to the error of the initial state $\hat{x}_0(i)$. If there is the bigger error of $\hat{x}_0(i)$, $P_0^x(i,i)$ should be set to the bigger value too. Hence, $P_0^x(2,2)$ is set to 0.1 and $P_0^x(1,1)$ is set very closely to zero. Similarly, Q_k^x is a 2×2 symmetric positive definite matrix. The initial values of $Q_k^x(i,i)$ are set correspondingly to the level of system noise $w_k(i)$. If there is the higher level of noise $w_k(i)$, $Q_k^x(i,i)$ should be set to the higher value too. R_k^x is a 1×1 symmetric positive definite matrix. The initial value of R_k^x is set correspondingly to the level of the measurement noise v_k. δ_x is a performance boundary related to the model accuracy; smaller δ_x means a more accurate state-space model. If the state-space model is believed to be accurate, δ_x should be set very closely to zero. With the high accuracy mode based on online parameter identification, δ_x is selected to be less than 1. S_k^x is a 2×2 symmetric positive definite matrix. The initial values of $S_k^x(i,i)$ are determined on the basis of the degree of interest in the states. If one state $x_k(i)$ is more interested than the other states, $S_k^x(i,i)$ corresponding to $x_k(i)$ should be set to the bigger value. The state of the SoC is the focus of this study, thus $S_k^x(2,2)$ is set to 10 and $S_k^x(1,1)$ is set to 1. In the same way, the parameters can be tuned in the parameter estimate module.

IV. Verification and Discussions

A. Experimental Setup

The battery test bench is set up to acquire the experimental data and is shown in Fig. 4, which consists of a battery testing system (Arbin BT2000), three thermal chambers, a computer, and the batteries or battery pack. The battery testing system regulates battery charging and discharging with the established

TABLE III
THE SPECIFICATIONS OF THE CELLS AND ITS RELATED PREPARATION TESTS

Battery types	LMO	NCM1
nominal capacity (Ah)	35	2
Rated voltage (V)	3.7	3.6
Cut-off voltage (V)	4.2/3.0	4.1/3.0
Preparation tests	Static capacity test, hybrid pulse test, OCV test, and driving cycles test at 25 °C	Static capacity tests; OCV tests; and dynamic stress tests at 10, 25, and 40 °C and at the room temperature

TABLE IV
COEFFICIENTS OF OCV FUNCTIONS–UOC(Z)

α_0	α_1	α_2	α_3	α_4	α_5	α_6
4.827	−2.197	2.529	−1.128	0.02153	0.5104	−0.01409

strategy and collects currents and voltages, which are then sent to the computer. The computer is used for the human–machine interface and experimental data storage. The thermal chambers are used to control the environment during the test.

The accuracies of the voltage and current acquisition of Arbin BT2000 are about 0.05%. The batteries under test in this study include two kinds of lithium-ion batteries and their specifications and related preparation tests are shown in Table III, where the LMO means the $LiMn_2O_4$ battery and the NCM means the $Li(NiCoMn)O_2$ battery. One NCM battery (NCM1) is used in the verification process while the other NCM battery (NCM2) is used in the battery-in-loop verification.

The capacity test is to obtain the battery capacity prepared for the hybrid pulse test; the hybrid pulse test is used to determine the battery parameters off-line; both the driving cycles and dynamic stress test (DST) are used for verification and comparison of the aforementioned estimation algorithms.

In Section IV-B, we use the data of LMO battery to compare three algorithms that are the HIF, the EKF, and the dual HIF for the SoC estimation with the known battery capacity, which aims to prove the superiority of the HIF and the dual HIFs. In Section IV-C, we use the data of NCM battery to demonstrate that the multiscale dual HIF can provide more accurate estimation of SoC and capacity than the single-scale dual HIF and EKF as well as the multiscale dual EKF.

1) Data of LMO Battery: We can obtain the cell capacity by means of the capacity test, the OCV function $U_{oc}(z)$ in (25) with the coefficients shown as Table IV and the other parameters with the data of the hybrid pulse test and the OCV test. They are all used to estimate the cell state with the off-line EKF and HIF.

The battery in EVs will be fully charged but not be fully discharged because of the endurance mileage and the battery life, the SoC in the range of 100% to 20% is selected in this study. The driving cycles is used to simulate the typical urban driving cycle of EVs. Based on the Arbin data-logger, we apply the current profile based on the driving cycles to the battery, as shown in Fig. 5(a), and obtain the corresponding trajectory of

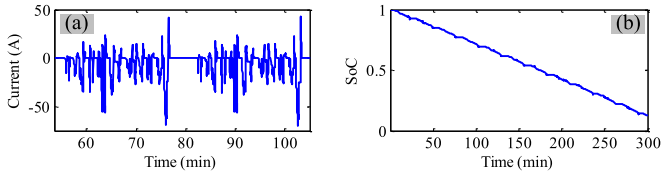

Fig. 5. Test results of driving cycles: (a) current profile (zoom) and (b) corresponding response SoC.

TABLE V
CELL CAPACITY AT DIFFERENT TEMPERATURES

Temperature	10 °C	25 °C	45 °C	Room
Capacity (Ah)	2.0568	2.0806	2.1165	2.0960

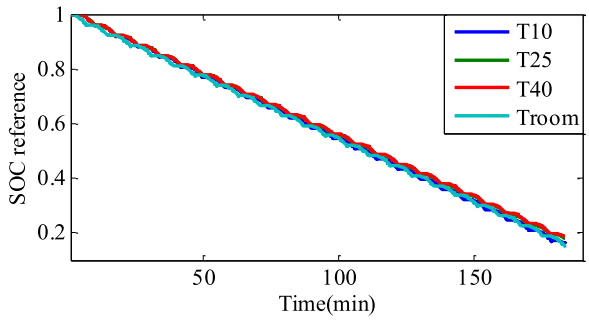

Fig. 6. SoC reference trajectory at 10 °C (T10), 25 °C (T25), 40 °C (T40), and the room temperature (Troom).

SoC, as shown in Fig. 5(b), which is used as a reference (or true) SoC, where it is assumed that the coulomb efficiency is 100%.

2) Data of NCM1 Battery: Similarly, we can obtain the cell capacities at 10, 25, and 40 °C and the room temperature by means of the capacity tests as shown in Table V. With the data of the OCV tests at 10, 25, and 40 °C and the room temperature, we obtain the OCV functions $U_{oc}(C_a, z)$ with different cell capacities. Fig. 6 shows the SoC trajectories corresponding to the DSTs at 10, 25, and 40 °C and the room temperature.

The experimental data at three different temperatures of 10, 25, and 40 °C are used to verify the estimation accuracy of the multiscale dual HIF algorithm. The experimental data at room temperature is used to validate its prediction accuracy and stability.

B. Evaluation of HIF, EKF, and Dual HIF

Based on the experimental data of the LMO battery, the HIF, EKF, and dual HIF are used to estimate SoC when the initial value of SoC is erroneous and capacity is known. Their estimation results are compared in terms of the accuracies of the SoC and terminal voltage, the error bound of the SoC and their convergence rates.

1) Evaluation of HIF and EKF: With the off-line parameters, the HIF and the EKF are used to estimate SoC when the initial value is erroneous. The terminal voltage and SoC estimation results of the HIF and the EKF with the erroneous initial SoC (80%) are plotted in Fig. 7.

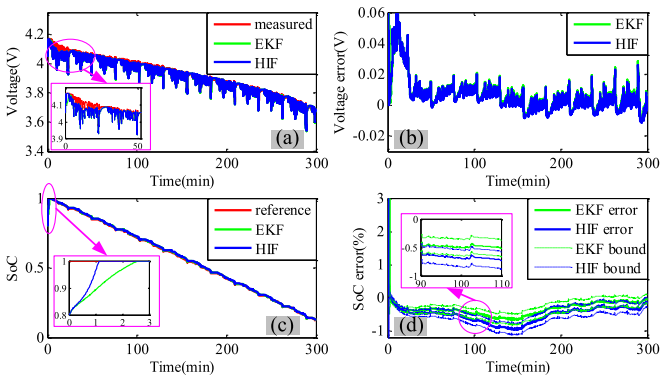

Fig. 7. Comparison results of EKF and HIF: (a) estimated and measured voltage and (b) corresponding error; (c) estimated and reference SoC; and (d) corresponding error.

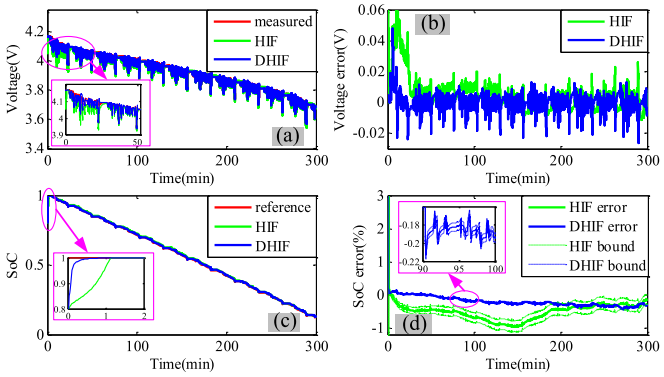

Fig. 8. Comparison results of HIF and DHIF: (a) estimated and measured voltage and (b) corresponding error; (c) estimated and reference SoC; and (d) corresponding error.

It shows that the absolute value of voltage estimation error is less than 0.06 V and the absolute value of SoC estimation error is less than 1% when the SoC is estimated with the HIF. When the SoC is estimated with the EKF, it has very similar estimation accuracy to the HIF. However, the HIF has higher convergence rate than the EKF, namely, the HIF can reach the true values in 70 s, while the EKF takes 140 s.

2) Evaluation of HIF and Dual HIFs: From the observation of the aforementioned results, it is found that the fitting errors of battery terminal voltage are slightly high due to the inaccurate model with the parameters determined off-line. This inaccurate model also affects the measurement-update procedure for the SoC estimation. If we pay more attention to the SoC estimation accuracy, it may result in large errors of terminal voltage or other states, which will, in turn, cause the large auto-covariance and error bound and, thus, increase the uncertainty of the SoC estimation. The dual HIF (DHIF) can provide online estimation of the model parameters, which can reduce the fitting errors of terminal voltage and improve the SoC estimation. The terminal voltage and SoC estimation results of the HIF and DHIF with the erroneous initial SoC (80%) are plotted in Fig. 8.

It shows that the DHIF has the absolute value of voltage estimation error less than 0.02 V in most of time except the initial period and the absolute value of the SoC estimation error less than 0.5%. It is far superior to the HIF in terms of the estimation accuracies of the SoC and terminal voltage, the error bound of the SoC, and the convergence rate.

The comparison of the numerical results for the EKF, HIF, and DHIF is summarized in Table VI.

TABLE VI
COMPARISON OF EKF, HIF, AND DHIF WITH ERRONEOUS INITIAL SOC SETTING OF 80%

	RMS Error of Voltage (mV)	RMS Error of SoC (%)	Bounds Error of SoC (%)	Convergence Time of SoC (s)
EKF	12.99	1.04	0.20	140
HIF	12.23	0.96	0.20	70
DHIF	5.59	0.35	0.02	30

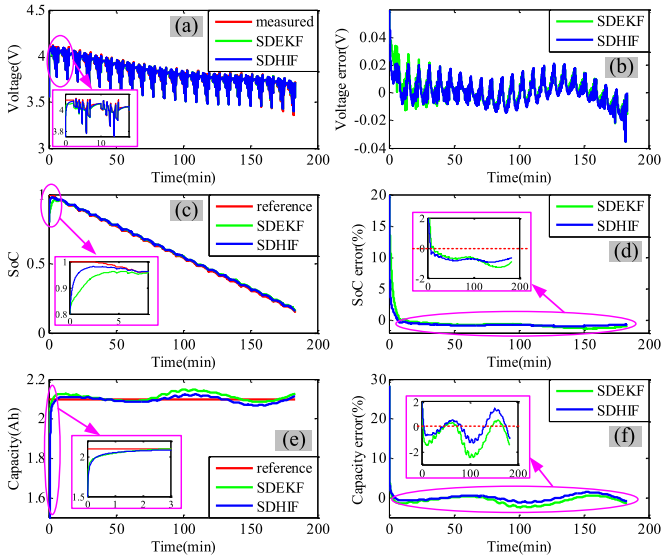

Fig. 9. Results of SDHIF and SDEKF: (a) estimated and measured voltage and (b) corresponding error; (c) estimated and reference SoC and (d) corresponding error; (e) estimated and reference capacity; and (f) corresponding error.

C. Single-Scale Dual HIF and EKF and Multiscale Dual HIF and EKF for SOC Estimation and Capacity

Based on the experiment data of the NCM1 battery, the multiscale dual HIF ($L = 60$), the single-scale dual HIF ($L = 1$), the single-scale dual EKF ($L = 1$), and the multiscale dual EKF ($L = 60$) are utilized to estimate the SoC and capacity when the initial value of SoC and capacity are erroneous. Their results will be evaluated in terms of the estimation accuracies of the SoC, capacity, and terminal voltage as well as the convergence rate of the SoC and capacity.

1) Comparison Between Dual HIFs and Dual EKF: With the DST data at room temperature, the estimation results of the single-scale dual HIF (SDHIF) and the single-scale dual EKF (SDEKF) are plotted in Fig. 9 and the estimation results of the multiscale dual HIF (MDHIF) and the multiscale dual EKF (MDEKF) are plotted in Fig. 10, where the erroneous initial SoC is set to 80% and the erroneous initial capacity is set to

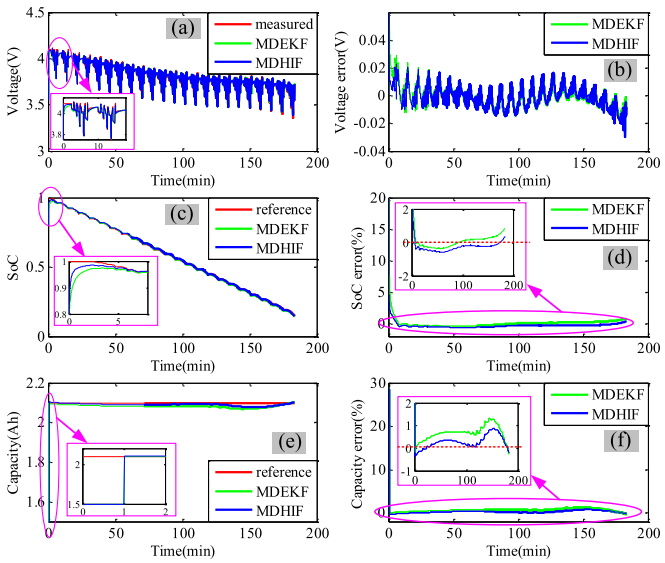

Fig. 10. Results of MDHIF and MDEKF: (a) estimated and measured voltage and (b) corresponding error; (c) estimated and reference SoC and (d) corresponding error; (e) estimated and reference capacity; and (f) corresponding error.

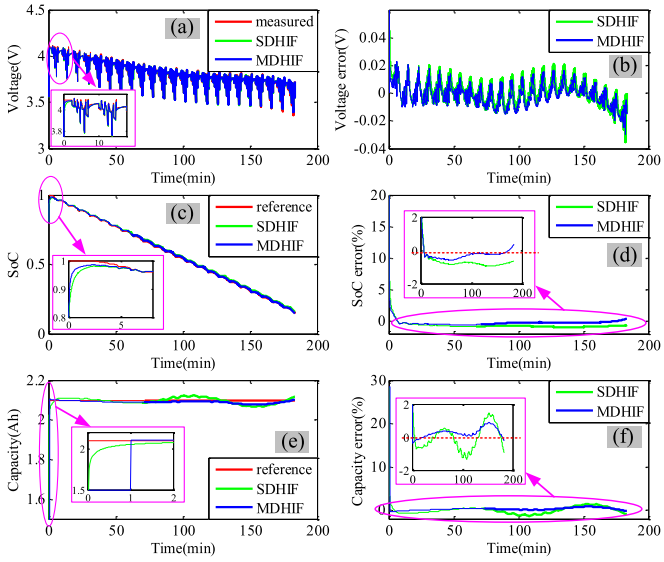

Fig. 11. Results of SDHIF and MDHIF: (a) estimated and measured voltage and (b) corresponding error; (c) estimated and reference SoC and (d) corresponding error; (e) estimated and reference capacity; and (f) corresponding error.

1.5 Ah while in fact the true SoC is 100% and the true capacity is about 2 Ah.

Fig. 9(a) shows the measured voltages and the estimated terminal voltages from both SDHIF and SDEKF, and Fig. 9(b) shows that their estimation errors both are within 0.04 V. But, SDHIF's precision is higher than SDEKF between 0 and 30 min, which indicates that SDHIF is more stable than SDEKF with the erroneous initial values. Fig. 9(c) and (d) indicates the SoC estimation errors of SDHIF can not only converge to the reference value in 5 min but also maintain within 1% after convergence, and SDEKF has obviously lower convergence rate than SDHIF. Fig. 9(e) shows the reference and estimated capacities from both SDHIF and SDEKF, and Fig. 9(f) indicates their capacity estimation errors. They both can converge to the reference values within 2 min. Fig. 9(f) indicates that the capacity estimation errors obtained from SDHIF can keep in 2% and remain stable around 0% while the capacity estimation errors obtained from SDEKF go beyond 2% at about 100 min and have an increasing trend to negative half axis direction. The earlier analyses indicate that SDHIF has better robustness and higher estimation accuracy than SDEKF.

Similarly, Fig. 10(a) shows the measured and estimated terminal voltages from both MDHIF and MDEKF, and Fig. 10(b) shows their voltage estimation errors; these errors are slightly less than 0.03 V. The estimated terminal voltage from MDHIF is more stable than MDEKF with the erroneous initial value. Fig. 10(c) shows the reference and estimated SoCs from both MDHIF and MDEKF, and Fig. 10(d) indicates their estimation errors. They both can not only converge to the reference values in 5 min but also keep in 1% after convergence. Fig. 10(c) also indicates MDHIF has higher convergence rate than MDEKF. Fig. 10(e) indicates the reference and estimated capacities from both MDHIF and MDEKF, and Fig. 10(f) indicates their estimation errors; they both can converge to the reference value in 1 min. After convergence, MDHIF can keep the errors in 1%, while MDEKF can keep the errors in 2%. The earlier analyses indicate MDHIF has better robustness and higher estimation accuracy than MDEKF.

2) Evaluation of Multiscale and Single-Scale Dual HIFs: With the DST data at room temperature, the estimation results of SDHIF and MDHIF with the erroneous initial SoC (80%) and the erroneous initial capacity (1.5 Ah) are plotted in Fig. 11. Fig. 11(a) and (b) shows the measured and estimated terminal voltages from SDHIF and MDHIF and their voltage estimation errors, respectively. It can be seen from Fig. 11(b) that MDHIF has slightly smaller estimation errors than SDHIF. Furthermore, MDHIF has faster convergence rate than SDHIF, as shown in Fig. 11(c). Fig. 11(d) indicates the SoC estimation errors from MDHIF are less than those from SDHIF all the time. Fig. 11(e) shows the estimated capacity from MDHIF converges to the reference value faster than those from SDHIF, where the former only takes one update and the latter takes many updates and more time. Fig. 11(f) indicates the capacity estimation errors from MDHIF are less than those from SDHIF all the time. The aforementioned comparisons show that the multiscale algorithm has better robustness and higher estimation accuracy than a single-scale one.

The battery parameters change slowly, but a single-scale algorithm frequently updates the parameters, which reduce the stability of the parameters. This will weaken the state correction based on the terminal voltage and affect the state estimation accuracy, which, in turn, affects the estimation accuracy of the parameters. As a result, the single-scale algorithm greatly reduces the estimation accuracy and stability, which is consistent with the experimental results, as shown in the earlier analysis. Thus, the multiscale algorithm is superior to the single-scale algorithm. The comparison of the numeric results obtained from the single-scale and multiscale algorithms is shown in Table VII.

TABLE VII
COMPARISON OF SINGLE-SCALE AND MULTISCALE ALGORITHMS

	RMS Error of Voltage (mV)	RMS Error of SoC (%)	RMS Error of Capacity (%)	SimulationTime (s)
Single-scale dual EKF	11.08	1.59	1.24	2.26
Single-scale dual HIF	11.47	1.07	0.87	2.77
Multiscale dual EKF	10.37	0.90	0.79	1.58
Multiscale dual HIF	9.38	0.64	0.47	1.99

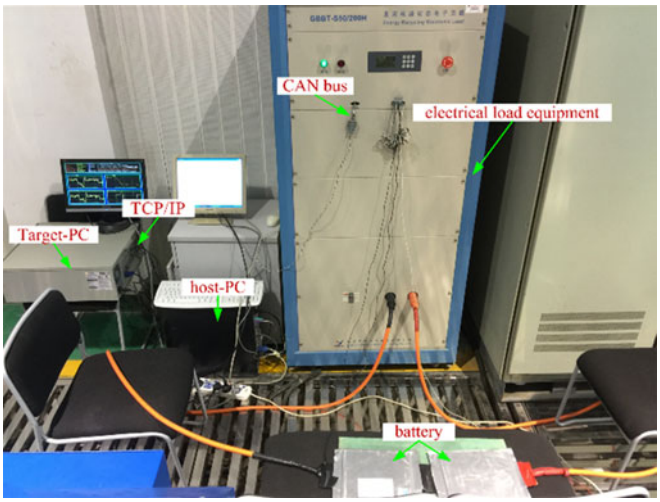

Fig. 12. Physical map of battery-in-loop test bench.

V. BATTERY-IN-LOOP VERIFICATION

In order to further verify the estimation accuracy of the SoC and capacity, the battery-in-loop test bench based on xPC target is designed to closely simulate EV operation conditions for a real-time validation of the multiscale dual estimation algorithms.

A. Battery-in-Loop Test Bench

The battery-in-loop test bench is shown in Fig. 12. It consists of host-PC, Target-PC, electrical load equipment, I/O interface, and software part. The host-PC is used to design the models and generate the executable codes in Real Time Workshop in MATLAB/Simulink. These codes will be downloaded to the Target-PC through TCP/IP. The target-PC executes the codes to control and operate the electrical load equipment by CAN bus. The electrical load equipment regulates battery charging and discharging with the established strategy and collects currents and voltages, which are then sent to the Target-PC through CAN bus. In the Target-PC, these data of currents and voltages is further imported to the model downloaded from host-PC for further calculation [27].

With the continuous operations in Target-PC, this bench can achieve the online estimation of the SoC and capacity in the real working environment of the battery in EVs to the maximum extent. It should be noted that the accuracies of the voltage and current acquisition of electrical load equipment are about 0.5%, which is aligned with the accuracy of the current and voltage acquisition in real EVs [27].

Considering that the minimum measurement voltage of electrical load equipment is 5 V, which is higher than the voltage of a single battery, we select two similar batteries in series for testing and the specifications of the selected two batteries is shown in Table VIII.

TABLE VIII
SPECIFICATION OF SELECTED TWO BATTERIES IN BATTERY-IN-LOOP TEST

Battery Species	NCM2
Nominal capacity (Ah)	25
Rated voltage (V)	3.6
Cut-off voltage (V)	4.15/2.5

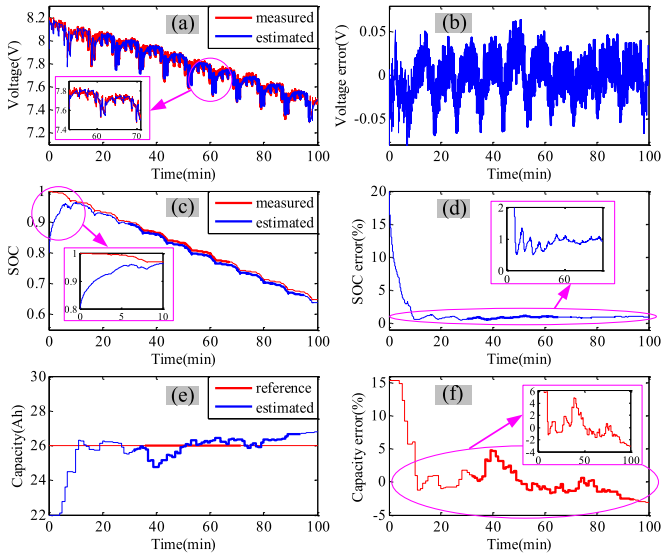

Fig. 13. Results of multiscale dual estimation of SoC and capacity in battery-in-loop test: (a) comparison of estimated and measured voltage; (b) model error, (c) comparison of estimated and reference SoC; (d) SoC estimation error; (e) comparison of estimated and reference capacity; and (f) capacity estimation error.

B. Analysis and Evaluation of Multiscale Dual Estimation of SoC and Capacity

In the case of the battery fully charged, the Target-PC loads the DST testing current profile to the batteries using the electrical load equipment. The multiscale dual estimation algorithm based on MDHIF downloaded from host-PC with the erroneous initial value of the SoC and capacity is used to estimate the SoC and capacity in real time. The online estimation results of terminal voltage, SoC and capacity are plotted in Fig. 13.

It shows the absolute value of voltage estimation error is slightly less than 0.06 V, and the SoC and capacity estimation errors can converge to the reference value gradually and stabilize in 2% and 4%, respectively. The results demonstrate that the proposed MDHIF meets the actual needs and verifies its suitability of EV applications.

VI. Conclusion

This paper proposes a multiscale dual HIFs for the SoC and capacity estimation. First, the dual HIF is compared with the HIF and the EKF for the SoC estimation at the erroneous initial SoC and known battery capacity based on the experimental data of the LMO battery. The results indicate the dual HIF has the best performance and its SoC estimation can converge to the true value within 30 s while keeping the high accuracy within 0.5%. Second, the multiscale dual HIF is compared with the single-scale dual HIF and EKF as well as the multiscale dual EKF for the SoC and capacity estimation at the erroneous initial SoC and capacity based on the experimental data of the NCM battery. The results show that the multiscale dual HIF has the best robustness and estimation accuracy. Its SoC and capacity estimation can converge to the true values in 5 and 1 min, respectively, while maintaining the high accuracy within 1%. Finally, the stability and the accuracy of multiscale dual HIFs for battery SoC estimation are verified by the battery-in-the-loop approach.

References

[1] G. Ren, G. Ma, and N. Cong, "Review of electrical energy storage system for vehicular applications," *Renew. Sustain. Energy Rev.*, vol. 41, pp. 225–236, 2015.

[2] A. Barré, B. Deguilhem, S. Grolleau, M. Gérard, F. Suard, and D. Riu, "A review on lithium-ion battery ageing mechanisms and estimations for automotive applications," *J. Power Sources*, vol. 241, pp. 680–689, 2013.

[3] L. Maharjan, S. Inoue, H. Akagi, and J. Asakura, "State-of-charge (SOC)-balancing control of a battery energy storage system based on a cascade PWM Converter," *IEEE Trans. Power Electron.*, vol. 24, no. 6, pp. 1628–1636, Jun. 2015.

[4] H. Wang, M. Muneeb Ur Rehman, M. Evzelman, and R. Zane, "SIMULINK based hardware-in-the-loop rapid prototyping of an electric vehicle battery balancing controller," in *Proc. Control Model. Power Electron.*, 2015, pp. 1–6.

[5] M. Einhorn, F. V. Conte, C. Kral, and J. Fleig, "A method for online capacity estimation of lithium ion battery cells using the state of charge and the transferred charge," *IEEE Trans. Ind. Appl.*, vol. 48, no. 2, pp. 734–741, Mar./Apr. 2012.

[6] K. S. Ng, C.-S. Moo, Y.-P. Chen, and Y.-C. Hsieh, "Enhanced coulomb counting method for estimating state-of-charge and state-of-health of lithium-ion batteries," *Appl. Energy*, vol. 86, pp. 1506–1511, 2009.

[7] H. Chaoui, N. Golbon, I. Hmouz, R. Souissi, and S. Tahar, "Lyapunov-based adaptive state of charge and state of health estimation for lithium-ion batteries," *IEEE Trans. Ind. Electron.*, vol. 62, no. 3, pp. 1610–1618, Mar. 2015.

[8] T. Kim, W. Qiao, and L. Qu, "Real-time state of charge and electrical impedance estimation for lithium-ion batteries based on a hybrid battery model," in *Proc. Appl. Power Electron. Conf. Expo.*, 2013, pp. 563–568.

[9] I.-S. Kim, "Nonlinear state of charge estimator for hybrid electric vehicle battery," *IEEE Trans. Power Electron.*, vol. 24, no. 4, pp. 2027–2034, Jul. 2008.

[10] M. Charkhgard and M. Farrokhi, "State-of-charge estimation for lithium-ion batteries using neural networks and EKF," *IEEE Trans. Ind. Electron.*, vol. 57, no. 12, pp. 4178–4187, Dec. 2010.

[11] P. Singh, R. Vinjamuri, X. Wang, and D. Reisner, "Design and implementation of a fuzzy logic-based state-of-charge meter for Li-ion batteries used in portable defibrillators," *J. Power Sources*, vol. 162, no. 2, pp. 829–836, 2006.

[12] J. C. A. Anton, P. J. G. Nieto, C. B. Viejo, and J. A. V. Vilan, "Support vector machines used to estimate the battery state of charge," *IEEE Trans. Power Electron.*, vol. 28, no. 12, pp. 5919–5926, Dec. 2013.

[13] H. Aung, K. S. Low, and S. T. Goh, "State-of-charge estimation of lithium-ion battery using square root spherical unscented Kalman filter (Sqrt-UKFST) in nanosatellite," *IEEE Trans. Power Electron.*, vol. 30, no. 9, pp. 4774–4783, Sep. 2015.

[14] J. Meng, G. Luo, and F. Gao, "Lithium polymer battery state-of-charge estimation based on adaptive unscented Kalman filter and support vector machine," *IEEE Trans. Power Electron.*, vol. 31, no. 3, pp. 2226–2238, Mar. 2016.

[15] R. Banavar, "A game theoretic approach to linear dynamics estimation," *Ph.D. dissertation, Univ. Texas, Austin*, TX, USA, May 1992.

[16] X. Shen, "Discrete H∞ filter design with application to speech enhancement," in *Proc. IEEE Int. Conf. Acoust., Speech Signal Process.*, 1995, vol. 2, pp. 1504–1507.

[17] H. K. Sahoo, P. K. Dash, N. P. Rath, and R. Kant, "Estimation of power quality using complex H∞ filter," in *Proc. Int. Conf. Power Syst.*, 2009, no. 3, pp. 1–6.

[18] K. Ramakrishnan and G. Ray, "Robust H∞ filter design for a class of uncertain systems with time-varying state-delays," in *Proc. Int. Conf. Electr. Comput. Eng.*, 2012, pp. 775–778.

[19] I. Vitanov and N. Aouf, "Fault detection and isolation in an inertial navigation system using a bank of unscented H∞ filters," in *Proc. UKACC Int. Conf. Control*, 2014, pp. 250–255.

[20] E. Abraham and E. C. Kerrigan, "Lower-order H∞ filter design for bilinear systems with bounded inputs," *IEEE Trans. Signal Process.*, vol. 63, no. 4, pp. 895–906, Feb. 2015.

[21] F. Zhang, G. Liu, L. Fang, and H. Wang, "Estimation of battery state of charge with H∞ observer: Applied to a robot for inspecting power transmission lines," *IEEE Trans. Ind. Electron.*, vol. 59, no. 2, pp. 1086–1095, Apr. 2012.

[22] M. Charkhgard and M. H. Zarif, "Design of adaptive H∞ filter for implementing on state-of-charge estimation based on battery state-of-charge-varying modelling," *IET Power Electron.*, vol. 8, no. 10, pp. 1825–1833, 2015.

[23] C. Unterrieder, R. Priewasser, S. Marsili, and M. Huemer, "Battery state estimation using mixed Kalman/H infinity, adaptive Luenberger and sliding mode observer," in *Proc. Veh. Power Propulsion Conf.*, 2013, pp. 71–76.

[24] H. Chaoui, A. Elmejdoubi, and H. Gualous, "Online parameter identification of lithium-ion batteries with surface temperature variations," *IEEE Trans. Veh. Technol.*, to be published, doi: 1109/TVT.2016.2583478.

[25] H. Rahimi-Eichi, F. Baronti, and M.-Y. Chow, "Online adaptive parameter identification and state-of-charge coestimation for lithium-polymer battery cells," *IEEE Trans. Ind. Electron.*, vol. 61, no. 4, pp. 2053–2061, 2014.

[26] F. Sun and R. Xiong, "A novel dual-scale cell state-of-charge estimation approach for series-connected battery pack used in electric vehicles," *J. Power Sources*, vol. 74, pp. 582–594, 2015.

[27] Y. Zhang, R. Xiong, H. He, and W. Shen, "A lithium-ion battery pack state of charge and state of energy estimation algorithms using a hardware-in-the-loop validation," *IEEE Trans. Power Electron.*, vol. 32, no. 6, pp. 4421–4431, Jun. 2017.

[28] J. T. B. A. Kessels, B. Rosca, H. J. Bergveld, and P. P. J. van den Bosch, "On-line battery identification for electric driving range prediction," in *Proc. Veh. Power Propulsion Conf.*, 2011, pp. 1–6.

[29] X. Tang, X. Mao, J. Lin, and B. Koch, "Capacity estimation for li-ion batteries," in *Proc. Amer. Control Conf.*, 2011, vol. 145, no. 2, pp. 947–952.

[30] S. Grolleau *et al.*, "Calendar aging of commercial graphite/LiFePO4 cell-Predicting capacity fade under time dependent storage conditions," *J. Power Sources*, vol. 255, pp. 450–458, 2014.

[31] J. Kim S. Lee, and B. H. Cho, "Complementary cooperation algorithm based on DEKF combined with pattern recognition for SOC/capacity estimation and SOH prediction," *IEEE Trans. Power Electron.*, vol. 27, no. 1, pp. 436–451, Jan. 2012.

[32] H. Dai, X. Wei, Z. Sun, J. Wang, and W. Gu, "Online cell SoC estimation of Li-ion battery packs using a dual time-scale Kalman filtering for EV applications," *Appl. Energy*, vol. 95, pp. 227–237, 2012.

[33] Y. Hu and Y.-Y. Wang, "Two time-scaled battery model identification with application to battery state estimation," *IEEE Trans. Control Syst. Technol.*, vol. 23, no. 3, pp. 1180–1188, May 2015.

[34] K. H. Low, H. Wang, and M. Y. Wang, "On the development of a real time control system by using xPC target: Solution to robotic system control," in *Proc. IEEE Int. Conf. Autom. Sci. Eng.*, 2005, pp. 345–350.

[35] W. C. Lee and D. Drury, "Development of a hardware-in-the-loop simulation system for testing cell balancing circuits," *IEEE Trans. Power Electron.*, vol. 28, no. 12, pp. 5949–5959, Dec. 2013.

[36] Y. He, W. Liu, and B. J. Koch, "Battery algorithm verification and development using hardware-in-the-loop testing," *J. Power Sources*, vol. 195, no. 9, pp. 2969–2974, 2010.

[37] Y. Ye, Y. Shi, and A. A.O. Tay, "Electro-thermal cycle life model for lithium iron phosphate battery," *J. Power Sources*, vol. 217, pp. 509–518, 2012.

[38] R. Xiong, F. Sun, Z. Chen, and H. He, "A data-driven multi-scale extended Kalman filtering based parameter and state estimation approach of lithium-ion polymer battery in electric vehicles," *Appl. Energy*, vol. 113, pp. 463–476, 2014.

Cheng Chen received the M.S. degree in vehicle engineering, in 2014, from Beijing Institute of Technology, Beijing, China, where he is currently working toward the Ph.D. degree in vehicle engineering.

His current research interests include the state estimation of battery and the application of the core algorithms in battery management system.

Rui Xiong (S'12–M'14–SM'16) received the M.Sc. degree in vehicle engineering and the Ph.D. degree in mechanical engineering from Beijing Institute of Technology, Beijing, China, in 2010 and 2014, respectively. He conducted scientific research as a joint Ph.D. student in the DOE GATE Center for Electric Drive Transportation at the University of Michigan, Dearborn, MI, USA, between 2012 and 2014.

Since 2014, he has been an Associate Professor in the Department of Vehicle Engineering, School of Mechanical Engineering, Beijing Institute of Technology, Beijing, China. In 2015, he was a Visiting Associate Professor in the Faculty of Science, Engineering and Technology, Swinburne University of Technology, Australia. He has conducted extensive research and authored more than 70 peer-reviewed articles. His research interests mainly include electrical/hybrid vehicles, energy storage, and battery management system.

Dr. Xiong received the Excellent Doctoral Dissertation from Beijing Institute of Technology in 2014, the first prize of Chinese Automobile Industry Science and Technology Progress Award in October 2015 and the second prize of National Defense Technology Invention Award in December 2016. He received the Best Paper Awards from the journal Energies in 2015. He is an Associate Editor of the *Energy, Ecology and Environment.* He serves on the Editorial Board of the *Energies*, Guest Editors of IEEE ACCESS and *Applied Energy.*

W. X. Shen (S'00–M'02) received the Ph.D. degree from the University of Hong Kong, Hong Kong, China, in 2002.

From 2002 to 2003, he was a Lecturer in Ngee Ann Polytechnic, Singapore. From 2003 to 2008, he was a Lecturer and then a Senior Lecturer in the School of Engineering, Monash University Malaysia. He was a Research Fellow for one year in the School of Electrical and Electronics Engineering, Nanyang Technological University, Singapore. He is currently an Associate Professor in Electrical Engineering in the Faculty of Science, Engineering, and Technology, Swinburne University of Technology, Hawthorn, Vic., Australia. His current research interests include electric vehicles, renewable energy, and power systems.